JOURNAL OF PROPULSION AND POWER
Vol. 12, No. 1, January–February 1996

Time-Marching Euler Analysis of Ducted-Propellers

R. Srivastava*
University of Toledo, Toledo, Ohio 43606

A time-accurate solution procedure and its application to ducted-propeller configuration is described in this article. Three-dimensional unsteady Euler equations are solved using a hybrid scheme to reduce the computational time and memory requirements. The solution procedure is applied to a ducted-propeller obtained by enclosing an eight-bladed SR7 advanced propeller within a duct with NACA 0003 airfoil cross section, operating in a steady axisymmetric flowfield. The performance characteristics are compared with other published numerical results. The effect of tip-gap is found to be significant on performance and flow characteristics.

Introduction

ADVANCED propellers are capable of extending the high propulsive efficiency of a propeller to relatively high cruise Mach numbers. However, these propellers have very poor noise characteristics. By enclosing the propeller within a duct, the pressure waves emanating from the propeller are shielded. This helps to reduce the noise of an unducted-propeller and also allows for underwing installation. For these reasons the ducted-propeller configurations are gaining more acceptance. By reducing the tip losses, the aerodynamic efficiency of the propeller may be increased, however, due to increased weight penalty and duct drag, the overall engine efficiency is somewhat lower than that for an unducted-propeller.

Several numerical techniques have been applied to unducted single-rotation and counter-rotation propellers and have been outlined in Refs. 1 and 2. These vary in complexity from simple Goldstein-type strip analysis to analyses that solve the Euler and Navier–Stokes equations, however, few numerical solutions have been attempted for ducted-propellers. Mainly, experimental efforts were made in the 1950s to investigate the ducted-propeller configurations. These efforts, directed towards low-speed applications due to large drag associated with the cowl at higher flight velocities, are documented in a review by Sacks and Burnell.[3] Wright,[4] using vortex sheet models, was the first to attempt numerical solution by providing a method for selecting design parameters for heavily loaded fans. Blade element theory was later used by Weir[5] for the design of a ducted-propeller.

Namba[6] developed an unsteady lifting surface analysis for three-dimensional ducted-rotors, with infinitely long duct. The duct solid surface boundary condition was incorporated using the Greens theorem. Recently, Williams et al.[7] have provided a solution procedure, using lifting surface panel method, for unsteady aerodynamic and aeroelastic analysis of single-rotation ducted-propellers. A flat plate duct of finite length and zero thickness is used in this analysis. Time-averaged three-dimensional Euler equations have been solved recently by Hall and Delaney[8] for steady aerodynamic analysis of ducted-propeller.

In the present work unsteady three-dimensional Euler equations are solved for a ducted advanced propeller configuration in a time-accurate fashion. Present work is an extension of the scheme for the unducted single-rotation[1] and counter-rotation geometry.[2] The primary objective of the present research is to develop a method for predicting the aeroelastic characteristics of ducted-propellers. This requires time-accurate analysis to account for arbitrary time-dependent motions of the blade and duct. As a first step towards using this solver for aeroelastic applications, the hybrid algorithm is applied here to the computation of the steady airloads and performance characteristics of the SR-7 single-rotation ducted-propeller.

Formulation

Solution Procedure

The solution procedure is described only briefly here. Interested readers are referred to Ref. 1 for a detailed description of the solution scheme. The Euler equations, in conservation form, in a Cartesian coordinate system can be written as

$$(\hat{q})_t + (\hat{E})_x + (\hat{F})_y + (\hat{G})_z = 0 \qquad (1)$$

where $\hat{q}$ is the vector containing conserved flow properties. $\hat{E}$, $\hat{F}$, and $\hat{G}$ are the nonlinear flux vectors that are functions of the vector $\hat{q}$, the subscripts denote the partial derivative of the vector. To simplify treatment of arbitrary geometries the Euler equations in Eq. (1) are transformed and recast in a generalized coordinate system. The transformed equations are then solved using a semi-implicit hybrid algorithm similar to the scheme by Rizk and Chaussee.[9] In the present scheme, in order to decrease the computational time, flux terms in two directions (streamwise ξ and azimuthal ζ), are treated implicitly while the radial η direction flux terms are treated semi-implicitly. The η derivative is obtained using the latest available values of the flow variables. The first-order-accurate Euler rule is used for time differencing and second-order-accurate central difference is used for spatial derivatives. Second/fourth-difference explicit dissipation and a second-order implicit dissipation are used to make the scheme stable and to reduce high-frequency errors. This leads to a block pentadiagonal system of equations coupling the implicitly treated nonlinear fluxes $\hat{E}$ and $\hat{G}$. As in the Beam–Warming algorithm[10] these fluxes are linearized about their values at the previous time level, resulting in a block pentadiagonal system of equations for the changes in the flow properties. This pentadiagonal system is approximately factored into two block tridiagonal system of equations and solved using the Thomas algorithm.

This method requires only two inversions of the block tridiagonal matrix, in the two implicit directions, as opposed to three for fully implicit schemes. It also reduces the memory

Presented as Paper 92-0522 at the AIAA 30th Aerospace Sciences Meeting and Exhibit, Reno, NV, Jan. 6–9, 1992; received Sept. 15, 1994; revision received Feb. 23, 1995; accepted for publication March 29, 1995.

*Senior Research Associate; currently Resident Research Associate, NASA Lewis Research Center, Cleveland, OH 44135. Member AIAA.

requirement by almost 50%, as only two time levels of information need to be stored at any given time, one of which needs to be only two dimensional. Using this technique the solver marches along the η direction solving the equations one η plane at a time. The marching direction is reversed after every time step in order to remove any dependency on the marching direction.

Because the duct and blades in relative motion must be analyzed, the flowfield is solved using multiblock grid technique, with only one grid and its solution being in the core memory at any given time. For an inviscid calculation, the duct, a body of revolution, could be treated either as a stator or a rotor (even though actual ducts are stators). This is possible because the inviscid fluid is insensitive to rotation of a body of revolution about its axis. In the present work the duct is treated as a rotor.

Initial and Boundary Conditions

In the present analysis freestream values are used as the initial conditions to start the solution procedure. The boundary conditions are applied explicitly after the governing equations have been solved for the interior flowfield. On the solid surfaces of blade, duct, and nacelle the no-penetration condition is applied as

$$V_b \cdot \boldsymbol{n} = 0 \tag{2}$$

where V_b is the relative velocity vector between fluid and solid at the surface and $\boldsymbol{n}$ is the outward unit vector normal to the surface. The tangential velocity components, the pressure, and the density are extrapolated from the interior of the domain.

For steady-state calculations all disturbances from the solid surface must propagate to infinity. On the subsonic inflow boundary one characteristic should be allowed to escape. Hence, one characteristic quantity is extrapolated and the other four quantities are fixed at the freestream value. At the subsonic outflow boundary, four characteristics should escape, thus, four fluid properties are extrapolated from the interior of the domain using the one-dimensional characteristics approximation, and the fifth quantity is fixed at the freestream value. These boundary conditions are based on the analysis presented in Ref. 11. For the downstream exit boundary the static pressure is obtained by solving the simple radial equilibrium equation[12]:

$$\frac{\partial p}{\partial r} = \frac{\rho v_\theta^2}{r} \tag{3}$$

where p is the pressure, ρ is the density, v_θ is the tangential velocity, and r is the radius. The other four characteristic quantities are extrapolated from the interior of the domain. The block interface fluid boundaries are updated by enforcing the second derivative of the fluid property to be zero across the boundary, at the boundary. These boundaries are also updated explicitly after the interior of the domain has been updated.

Results and Discussion

The SR7 propeller in the unducted configuration has been analyzed using the hybrid scheme for several flight configurations in Refs. 1 and 2. Comparisons with experimental data are also included. In the present work the scheme presented earlier has been applied to an SR7 ducted-propeller. The propeller is the standard eight-bladed SR7 advanced propeller with a duct of NACA 0003 airfoil cross section around it. The length of the duct is one radius and the duct is centered, lengthwise, about the pitch change axis and the tip-gap is 1.5%, unless otherwise noted. This particular configuration was chosen for demonstration purpose because other researchers[7,8] have also studied a similar configuration.

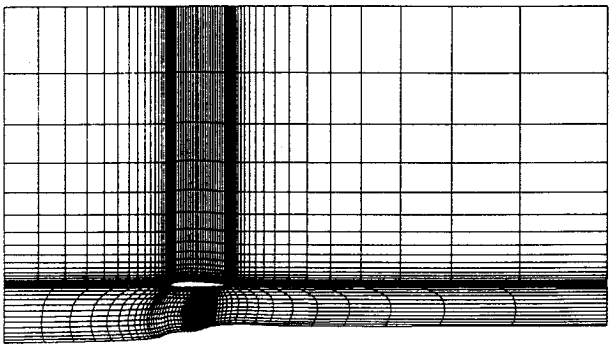

Fig. 1 Grid cross section in the streamwise plane.

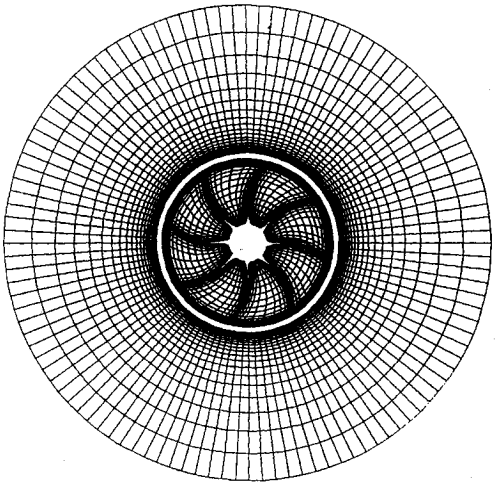

Fig. 2 Grid cross section in the azimuthal plane.

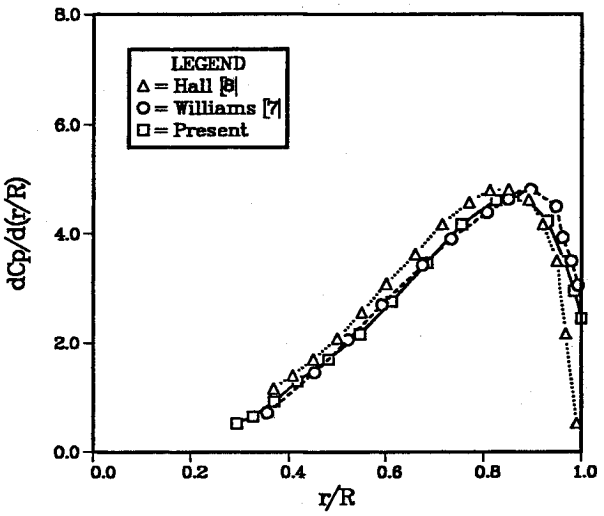

Fig. 3 Comparison of elemental power coefficient for the unducted SR7 eight-bladed propeller.

The grid used for the calculation has H-O topology, around the blade and the duct. Typical grid cross sections are shown in Figs. 1 and 2. For ease of calculation, the domain was radially blocked. The inner surface of the duct, the nacelle, and the blades constituted one block. The outer surface of the duct was part of the second block. The grid points are clustered near the solid surfaces in the direction normal to the surface.

The flowfield considered here is axisymmetric and steady, hence, only one blade passage is solved, enforcing the con-

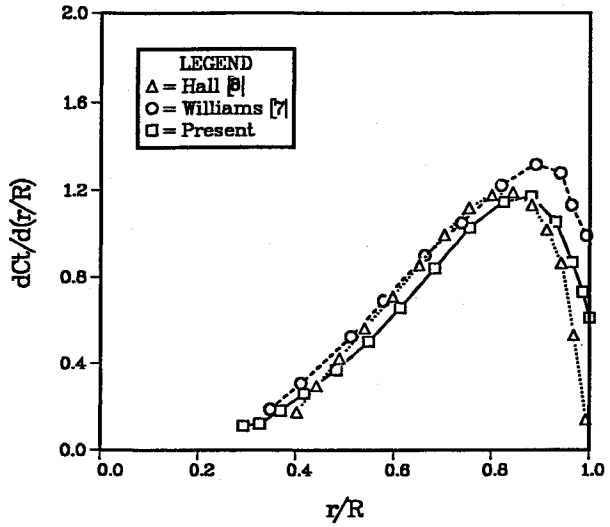

Fig. 4 Comparison of elemental thrust coefficient for the unducted SR7 eight-bladed propeller.

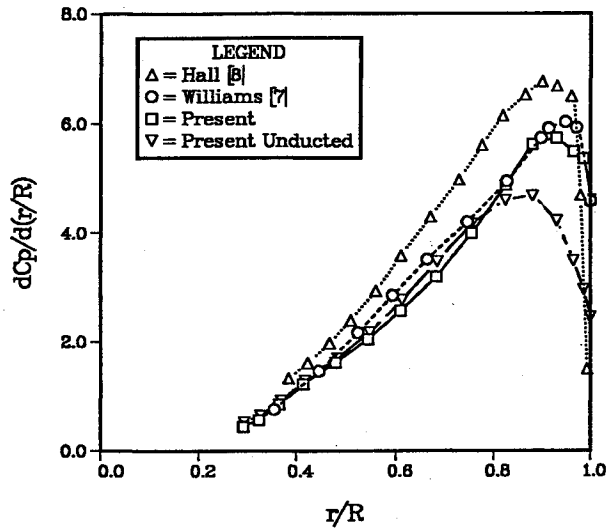

Fig. 5 Comparison of elemental power coefficient for the ducted SR7 eight-bladed propeller.

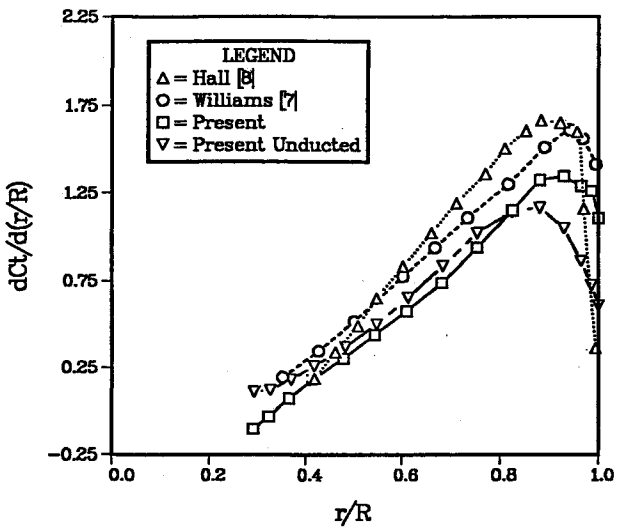

Fig. 6 Comparison of elemental thrust coefficient for the ducted SR7 eight-bladed propeller.

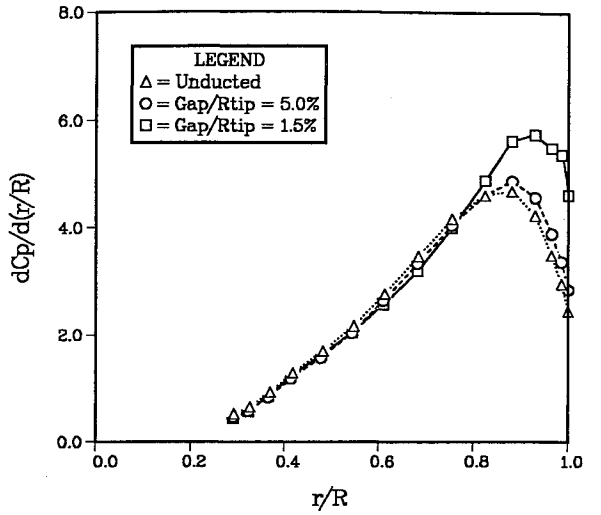

Fig. 7 Effect of tip-gap on elemental power coefficient for the ducted SR7 eight-bladed propeller.

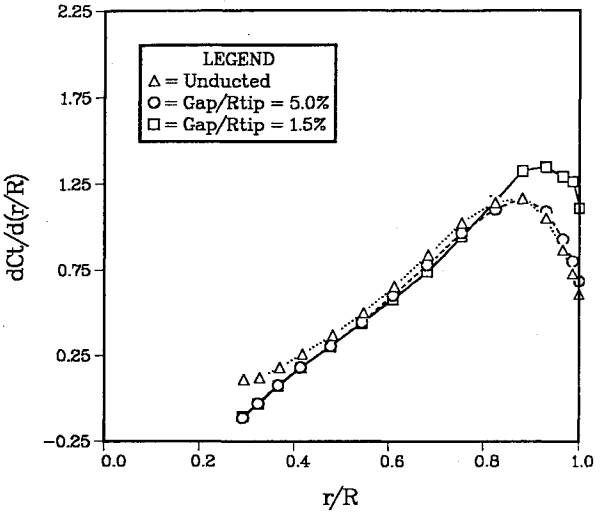

Fig. 8 Effect of tip-gap on elemental thrust coefficient for the ducted SR7 eight-bladed propeller.

ditions of symmetry. The propeller is operating at a flight Mach number of 0.7, advance ratio of 3.06, and blade setting angle of 60.2 deg. The blade loadings are obtained for both ducted and unducted geometry for the same flight parameters.

In Figs. 3 and 4 the spanwise variation of elemental power and thrust coefficients are compared, respectively, for the unducted configuration with two different numerical results presented in Ref. 7. The results have been reported in Refs. 7 and 8. It can be seen that the comparison is good for both the power and thrust coefficients between the three different schemes. Williams et al.,[7] however, predict a higher thrust coefficient in the tip region.

In Figs. 5 and 6 the spanwise distribution of the blade loading is compared for the ducted-propeller. Also shown in these figures is the spanwise loading of the unducted configuration obtained by the present scheme. All the three schemes show considerable increase in the loading, especially in the tip region for the ducted-propeller configuration. The results by Hall and Delaney, however, show a much higher increase in the loading on the inboard stations as well. It must be pointed out that the cross sections of the duct used in all three schemes are different. The choice of the duct cross section and the location of its leading edge could affect the spanwise distribution of the blade loading.

The effect of tip-gap is shown in Figs. 7 and 8. Blade loading distribution is shown for two different tip-gaps. Due to the cross section of the duct being a symmetric NACA airfoil, the gaps are not constant along the tip chord. Large tip-gaps do not have any significant effect on the blade loading. However, as the gap is reduced, the loading in the tip region increases significantly. For larger tip-gap ratios the duct changes the chordwise blade loading distribution near the tip, but the effect is not strong enough to increase the loading significantly. As the tip-gap is reduced the effect of duct becomes more significant. The pressure coefficients at two different radial locations are plotted for unducted and ducted configuration for a tip-gap of 1.5% (Fig. 9). It is evident from this figure that the presence of duct significantly changes the chordwise loading distribution on the blade. The effect is not restricted to outboard stations alone. On the inboard stations the pressure coefficient curve becomes more negative and the blade loading is reduced somewhat. This is because the local axial Mach number increases by approximately 8–10% as compared with unducted propeller. On the outboard station, however, the loading changes considerably. The trailing-edge section of the blade is more heavily loaded for the ducted propeller and also a strong shock is present near the trailing edge. No shock is evident for the unducted propeller. The loading on the blade will depend on the position and strength of the shock. For this reason the cross section and location of the duct may be important in achieving desired performance.

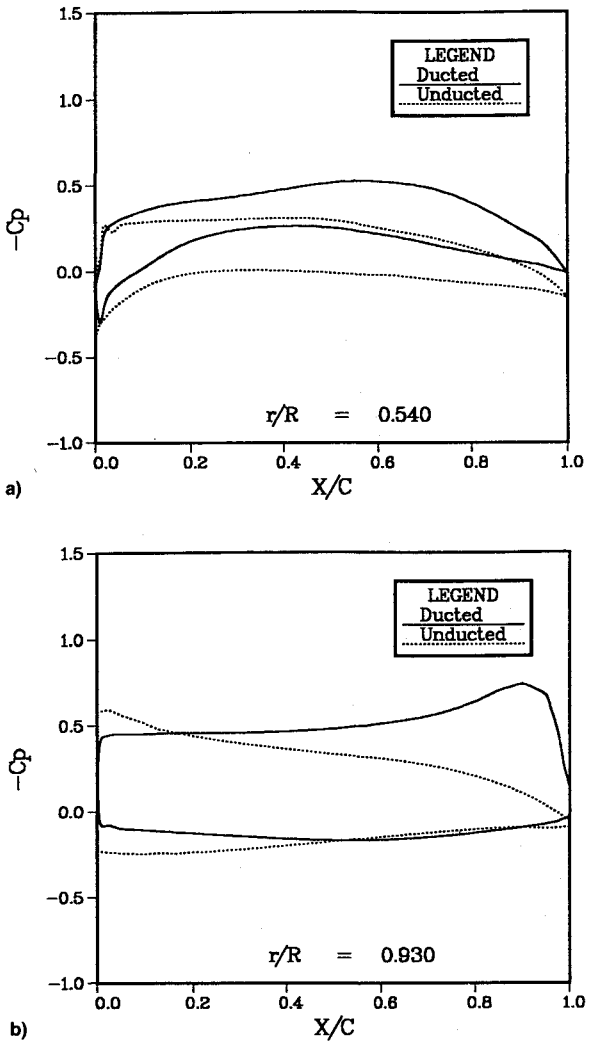

Fig. 9 Comparison of chordwise blade loading: a) midspan and b) tip region.

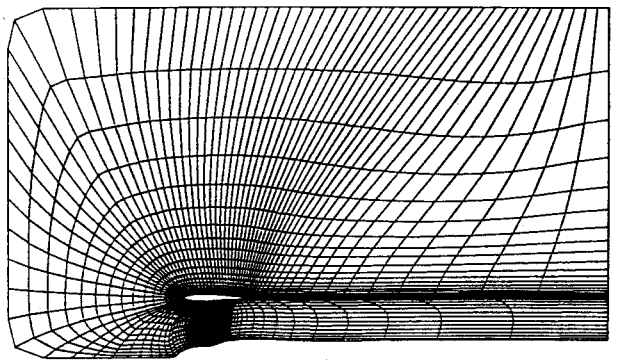

Fig. 10 C-grid topology in the streamwise plane.

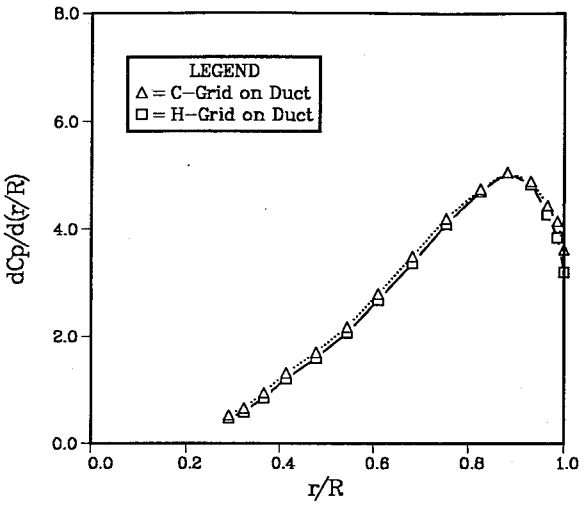

Fig. 11 Comparison of elemental power coefficient for the ducted SR7 eight-bladed propeller.

For the ducted propeller, it is not only important to accurately predict the effects of the duct on the blade, but also the loading on the duct itself. The loading on duct is important in estimating accurately the losses due to drag. This in turn makes the accurate prediction of pressure on the leading edge of the duct even more important. For this purpose a wrap-around C-grid topology around the leading edge of the duct is most suitable, especially since most practical ducts have large leading-edge radius. Hall and Delaney[8] have also used patched C-grid topologies around the duct in some of their calculations, for similar concerns. In this topology, again, the domain is blocked. The block containing the blades has the same H-O grid topology as in the previous case. The other block containing the leading edge of the duct and the outer surface of the duct has a C-grid topology. The grid in the streamwise plane is shown in Fig. 10. Some preliminary calculations using this topology have been carried out. Initial results are encouraging. A comparison of the spanwise loading of the blade using the two different topologies is shown in Fig. 11. The blade loading compares quite well, indicating that either grid topology can be successfully used for predicting the blade loadings. However, as the C-grid topology is expected to give better suction characteristics near the leading edge of the duct, this configuration will be used in future calculations.

All of the previous computations were performed on the Cray Y-MP computer at the NASA Lewis Research Center. A grid size of 80 × 18 × 15 was used for one blade passage of the block containing the blades. A grid size of 70 × 15 × 22 was used for one blade passage of the block containing the outer surface of the duct. The total memory and CPU time required per time step were 1.8 MW and 1.602 s, respectively.

Conclusions

A time-marching Euler solver has been developed and successfully applied to ducted propeller configurations. To reduce computer time and memory a hybrid solution technique has been used. The study showed good correlation with other numerical solutions. Effect of tip-gap was also studied and the analysis showed that large gaps, as expected, did not significantly change the blade loading. It was also observed that the effects of smaller tip-gap were not restricted to the tip region only. Pressure distribution, flow Mach number, and blade loading showed significant changes due to smaller tip-gap, even on inboard stations. The loading and flow characteristics changed significantly in the tip region with variation of tip-gap.

Acknowledgments

This work has been carried out under NASA Grant NAG3-730 from the NASA Lewis Research Center in Cleveland, Ohio. The author wishes to thank L. N. Sankar of the Georgia Institute of Technology, Atlanta, Georgia, for many valuable suggestions and discussions.

References

[1]Srivastava, R., Sankar, L. N., Reddy, T. S. R., and Huff, D. L., "Application of an Efficient Hybrid Scheme for Aeroelastic Analysis of Advanced Propellers," *Journal of Propulsion and Power*, Vol. 7, No. 5, 1991, pp. 767–775.

[2]Srivastava, R., and Sankar, L. N., "An Efficient Hybrid Scheme for the Analysis of Counter Rotating Propellers," *Journal of Propulsion and Power*, Vol. 9, No. 3, 1993, pp. 382–388.

[3]Sacks, A. H., and Burnell, J. A., "Ducted Propellers—A Critical Review," *Progress in Aeronautical Sciences Vol. III*, Pergamon, New York, 1962, pp. 87–135.

[4]Wright, T., "Evaluation of the Design Parameters for Optimum Heavily Loaded Ducted Fans," *Journal of Aircraft*, Vol. 7, No. 6, 1970, pp. 512–519.

[5]Weir, R. J., "Ducted Propeller Design and Analysis," Sandia National Lab., Sandia Rept., SAND87-2118, Albuquerque, NM, Oct. 1987.

[6]Namba, M., "Three-Dimensional Flows," *Aeroelasticity in Axial-Flow Turbomachines, Vol. 1, Unsteady Turbomachinery Aerodynamics*, edited by M. F. Platzer and F. O. Carta, AGARD-AG-298, March 1987.

[7]Williams, M. H., Cho, J., and Dalton, W. N., "Unsteady Aerodynamic Analysis of Ducted Fans," *Journal of Propulsion and Power*, Vol. 7, No. 5, 1991, pp. 800–804.

[8]Hall, E. J., and Delaney, R. A., "Investigation of Advanced Counterrotation Blade Configuration Concepts for High Speed Turboprop Systems," Final Rept., NASA CR-185217, April 1990.

[9]Rizk, Y. M., and Chaussee, D. S., "Three-Dimensional Viscous-Flow Computations Using a Directionally Hybrid Implicit-Explicit Procedure," AIAA Paper 83-1910, July 1983.

[10]Beam, R. M., and Warming, R. F., "An Implicit Factored Scheme for the Compressible Navier-Stokes Equations," *AIAA Journal*, Vol. 16, No. 4, 1978, pp. 393–401.

[11]Whitfield, D. L., Swafford, T. W., Janus, J. M., Mulac, R. A., and Belk, D. M., "Three-Dimensional Unsteady Euler Solutions for Propfans and Counter-Rotating Propfans in Transonic Flow," AIAA Paper 87-1197, June 1987.

[12]Horlock, J. H., *Axial Flow Turbines—Fluid Mechanics and Thermodynamics*, Robert Krieger, Malabar, FL, 1982, pp. 11–13, 148.